An Exploration of Radial Flow on a Rotating Blade in Retreating Blade Stall

Vrishank Raghav
Graduate Research Assistant

Narayanan Komerath*
Professor

Daniel Guggenheim School of Aerospace Engineering
Georgia Institute of Technology, Atlanta, GA

The nature of radial flow during retreating blade stall on a two-bladed teetering rotor with cyclic pitch variation is investigated using laser sheet visualization and particle image velocimetry in a low-speed wind tunnel. The velocity field above the retreating blade at 270° azimuth shows the expected development of a radially directed jet layer close to the blade surface in the otherwise separated flow region. This jet is observed to break up into discrete structures, limiting the spanwise growth of the radial velocity in the jet layer. The discrete structures are shown to derive their vorticity from the "radial jet" layer near the surface, rather than from the freestream at the edge of the separated region. The separation line determined using velocity data shows the expected spanwise variation. The results of this study are also correlated in a limited range of extrapolation to the phenomena encountered on a full-scale horizontal axis wind turbine in yaw.

Nomenclature

a_o	wind deficit factor
c	chord length, m
k	reduced frequency
R	rotor radius, m
Re	Reynolds number
r	radial/spanwise location, m
V_c	velocity component in the plane of the wind turbine, m/s
V_i	induced velocity for the rotor setup, m/s
V_n	velocity component normal to the wind turbine, m/s
V_r	radial velocity, m/s
V_{t_w}	tangential component of velocity to wind turbine blade, m/s
V_w	freestream velocity for wind turbine, m/s
V_∞	freestream velocity for rotor setup, m/s
x	chordwise location, m
z	axial location, m
α_{i_r}	induced angle of attack on rotor setup, deg
α_{i_w}	induced angle of attack on wind turbine, deg
α_{p_r}	blade pitch of rotor setup, deg
α_{p_w}	blade pitch of wind turbine, deg
α_r	angle of attack of rotor setup, deg
α_w	angle of attack of wind turbine, deg
Δt	time interval between pulses, s
γ	wind turbine yaw angle, deg
ψ	azimuthal position, deg
Ω	rotation rate, rad/s
ω	vorticity, 1/s
ω_f	flapping frequency, rad

Introduction

Retreating blade stall of a helicopter rotor is a primary limitation of the flight envelope. Blade stall is accompanied by sharp changes in pitch link loads and vibrations. Flow reattachment is delayed in a hysteresis loop which persists well into the fourth quadrant of the rotor disk. Although this phenomenon has been studied extensively, predicting the precise timing, extent, and hence the rotor phase of dynamic stall and reattachment remains elusive. Centrifugal effects on the boundary layer are expected to drive a strong radial flow, but experiments have not delineated the expected magnitude of these effects. The question "what is the role of radial flow on postdynamic stall lift and pitching moment evolution?" remains unanswered.

This work explores the radial velocity field during retreating blade dynamic stall. Experiments on a rotor in forward flight in a low-speed wind tunnel are used to derive conclusions that are relevant to the phenomena occurring on the retreating blades of a helicopter in high-speed forward flight. Particle image velocimetry (PIV) is used to investigate the detailed physics of the radial flow field on the retreating blades. In addition, the spanwise variation of the separation line is determined using velocity data. This work also discusses the correspondence between the wind tunnel test case and the relevant operating conditions on a full-scale horizontal axis wind turbine (HAWT) in yaw. It is shown that

*Corresponding author; email: Komerath@gatech.edu.

Presented at the 26th AIAA Applied Aerodynamics Conference, Honolulu, HI, August 18–21, 2008, and 2nd International Forum on Rotorcraft Multidisciplinary Technology, Seoul, Republic of Korea, October 19–20, 2009. Manuscript received October 2011; accepted January 2013.
Most figures in this paper are in color in the electronic version.

results from one type of test geometry can be used to infer details on the other.

The paper starts with a discussion on the phenomenon of dynamic stall. Most of the literature on explaining and predicting dynamic stall arises from interest in rotorcraft forward flight at high advance ratio, poststall maneuvering of combat aircraft, and operation of jet engine compressors at high stage pressure ratio. Research in this area has progressed from predictions and experiments on oscillating "airfoil sections" in wind and water tunnels (Refs. 1–4) to rotating blades with inflow and swept wings undergoing large excursions in angle of attack and roll. Extensive studies of dynamic stall on oscillating wings have been accomplished (Refs. 5–7) and numerical simulations have proceeded from inviscid formulations to full Navier–Stokes simulations (Refs. 8–10).

Prior work

Predicting the delayed onset of flow separation resulting from unsteady aerodynamics remains a tough challenge. This is especially true when the Reynolds number of the blade boundary layer is high enough so that the boundary layer upstream of separation is turbulent. In this case, studies show that stall initiation is a localized three-dimensional phenomenon, even if the blade itself has zero sweep and taper and is not rotating. Van Dommelen and Sten (Ref. 11) predicted the development of a singularity at the onset of separation, followed by focused sudden eruptions of boundary layer fluid into the outer stream, propagating the stall event. The precise timing of such events varies from cycle to cycle in the case of a helicopter in forward flight, although the flight condition is nominally steady. In the case of wind turbines, it has been observed in Ref. 12 that the dynamic stall vortex initiation strongly depends on local inflow angle. The above reasons make the timing of the dynamic stall difficult to predict and control.

In addition, according to Refs. 13 and 14 the three-dimensional effects that are unique to the rotating environment add critical concerns. The coupled effects of centrifugal and Coriolis forces in the rotating environment add more complexity to the flow characteristics (Ref. 15). Studies in Ref. 16 show that the dynamic stall region of wind turbine blades exhibits substantial radial pressure gradients. Radial acceleration appears to have a strong influence on poststall lift and pitching moment evolution. Moreover, deviations from the two-dimensional kinematics of dynamic stall vortex initiation on a wind turbine have been observed in Ref. 12. These three-dimensional influences include viscous interactions associated with rotational augmentation as well as inviscid ones like local sweep effects. McCroskey (Ref. 17) cites experimental evidence that the fluid in the stalled region does indeed move outward due to the centrifugal forces. Moreover, according to Corten (Ref. 16), the radial flow is pronounced on the inboard sections of a HAWT blade. Hence, understanding the nature of the near-surface flow under the influence of these coupled forces is crucial to predicting dynamic stall, to the accuracy needed for high advance ratio rotor design as well as wind turbine design.

Initial experiments at The Georgia Institute of Technology (Ref. 18) used a rotor in a hover facility, for the convenience in bringing the flow diagnostics close to the flow field. Transient stall was induced by an "inflow obstructer," which was a plate in the shape of a sector of a circular disk, placed axially upstream of the rotor. The rotor blade was set at a pitch angle well above the static stall angle of attack of the airfoil section. When operated as a rotor, the induced inflow would ensure that the blade remained unstalled. The pitch was increased by trial and error until it was just under the angle where the rotating blade would stall as it entered the region where the inflow was obstructed. Laser sheet visualization confirmed that stall was occurring over the blocked sector,

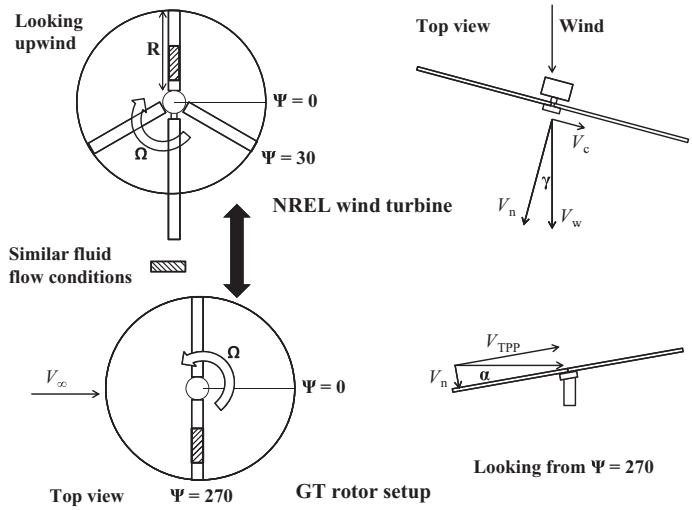

Fig. 1. Schematic representation of similar fluid flow conditions.

but the rotor was producing thrust elsewhere over the rotor disk. PIV data showed discrete structures developing in the velocity field when viewed in the axial-radial cross-flow section. These structures suggested a mechanism whereby the accelerated flow near the blade surface could be exchanged with the nearly stagnant flow away from the surface. In this particular experiment, the inflow obstruction was much more severe than what may be encountered in any practical engineered design of a rotating-blade device.

Following the "inflow obstructer" experiments, extensive PIV studies of the radial velocity field over a blade of a two-bladed teetering rotor in forward flight were conducted. The present paper is a revised, expanded, and integrated description of these studies (Refs. 19, 20).

Correspondence between the forward flight and yawed wind turbine cases

A small diversion is taken from the main thrust of this paper to identify the regions of flow similarity between the wind tunnel rotor dynamic stall experiment reported here and that on a full-scale HAWT. References 21 and 22 cite one limiter of the operating lifetime of horizontal axis wind turbines is the dynamic loading on blades and generators, sometimes far in excess of their design loads leading to fatigue failure. This dynamic loading is attributed to a variety of unsteady aerodynamic effects, including dynamic inflow, turbulence, wind shear, and dynamic stall. However, the problem of dynamic stall is of particular importance on wind turbines as the unsteady loads produced can be large enough to cause structural damage. Veers (Ref. 23) showed that a 30% error in prediction of airload leads to a 70% decrease in life expectancy of a wind turbine. Moreover, Huyer et al. in Ref. 24 showed that two-dimensional data on oscillating airfoils from wind tunnel tests are insufficient to construct a good estimate of the structural loading on a HAWT. Such data consistently underpredicted actual loading and power output (Ref. 25). Coton et al. (Ref. 26) reported that substantial differences have been observed in the pressure distribution of the inboard section of rotating wind turbine blades compared to two-dimensional models preceding dynamic stall.

In this paper the study was conducted on a rotor in forward flight. The hatched portions on the blades in Fig. 1 depict the portion of the blades that have similar flow conditions to a HAWT in yaw. The wind turbine case selected was the Grumman Wind Stream 33 Downwind HAWT used by the National Renewable Energy Laboratory in dynamic

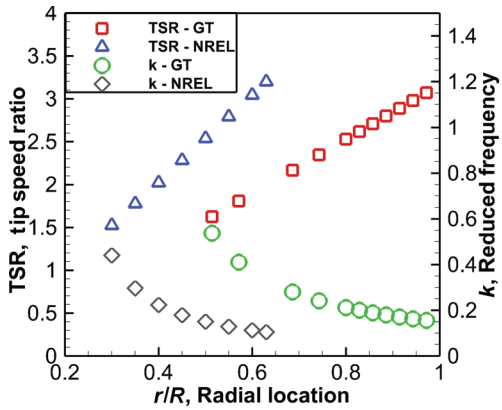

(a) Comparison of tip speed ratio and reduced frequency at $\psi = 270°$ ($\gamma = 30°$ for wind turbine)

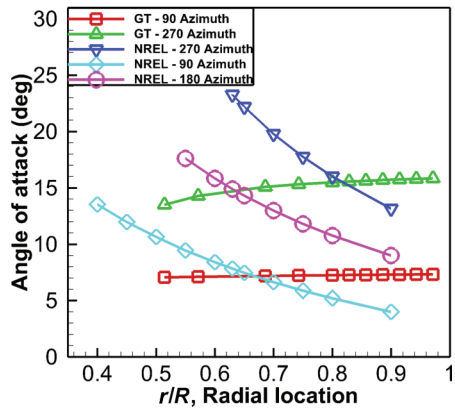

(b) Comparison of variation of angle of attack across the span at different azimuths ($\gamma = 30°$) for wind turbine

Fig. 2. Comparison of dynamic similarity parameters.

stall experiments (Ref. 24). For convenience of comparison to the rotor setup, the azimuth angle ψ has been defined *differently* from the regular convention. $\psi = 0$ starts at the right side of the turbine looking upwind (see Fig. 1).

The equations used to derive the dynamic similarity parameters are summarized in the Appendix. Figure 2 illustrates the similarities in the dynamic parameters of tip speed ratio, reduced frequency, and angle of attack. The rotor setup is in the same general operating regime as the wind turbine at yaw angles of $20°-30°$. Clearly, the reduced frequencies and tip speed ratios (as per the definition) are in the same regime. The range of angle of attack that the blades experience is comparable between setups. The rotating blades in each case are subjected to the same conditions; hence, the behavior and characteristics of the fluid flow over the blades should be similar.

Present scope and objectives

In this paper, the phenomenon of radial flow development over a rotor blade in the dynamic stall regime of forward flight is examined. The paper seeks to answer the question on whether the radial flow is of first-order significance to the prediction of dynamic stall.

Experimental Setup and Methodology

The experiment was conducted in the high advance ratio experimental setup constructed in the test section of the closed circuit John J. Harper 7 ft × 9 ft (2.13 m × 2.74 m) wind tunnel in the School of Aerospace Engineering at The Georgia Institute of Technology. The motor was positioned below the rotor with manually adjustable cyclic and collective pitch. To simplify the operations, a teetering rotor hub design was preferred.

Studies by Bousman (Refs. 27, 28) correlating flight data with predictions show that the event of primary interest in load prediction is the large excursion in blade pitching moment that accompanies the separation and convection of the dynamic stall vortex. One school of thought suggests that the timing of dynamic stall on full-scale helicopter rotor blades depends on shock–vortex interaction phenomena in the highly accelerated flow over the leading upper surface of the blade (Refs. 29, 30). The shock terminating this region may trigger or interact with the separation of the dynamic stall vortex. Thus it may be rightly extrapolated that experimental studies where the critical Mach number is not exceeded are irrelevant to predicting the stall line. But it should be noted that the flow field downstream of the stall line is incompressible, and studies in this region can be conducted ignoring compressibility. Furthermore, the large aspect ratio that is typical of helicopter and wind turbine blades is not essential to study the physics of the radial flow. This is because the stalled regions develop well inboard, eliminating aspect ratio effects. Thus a moderate aspect ratio, low tip Mach number test case is adequate for the purposes of studying the radial flow on a rotating blade in dynamic stall. These reasons form the basis for the design of the experimental setup used in this work.

Given the objectives and motivation of studying radial flow behind the stall line, a rotor rpm of 200 and a tunnel speed of 20 ft/s (6.1 m/s) was chosen. The operating advance ratio is 0.33, which is sufficient to induce dynamic stall as demonstrated in Ref. 20 by flow visualization. This condition results in a chordwise relative velocity of about 10.5 ft/s (3.21 m/s) at the rotor midradius at the 270° azimuth of the 35-inches (0.889-m) radius rotor. A collective of 10° and a cyclic of −5° were used to create a 15° pitch on the retreating blade at 270°. However, due to the flapping of the blade, the effective angle of attack observed on the retreating blade is 16.8°. These angles agree with the angles corresponding to the onset of dynamic stall for a NACA0012 airfoil as reported by McAlister et al. in Ref. 3. Further details of the facility and test are provided in Table 1.

Table 1. High Advance Ratio Facility rotor specifications

Description	Value	Unit
Rotor blade airfoil	NACA0012	
Blade mass total	1.747	kg
Blade span	0.622	m
Blade chord	0.178	m
Disc radius	0.889	m
Solidity	0.0895	
Precone	1.6	deg
Maximum collective	10	deg
Maximum cyclic	6.5	deg
Maximum TPP tilt	16	deg
Blade aspect ratio	3.49	
Motor	3.73	kW
Height	1.575	m

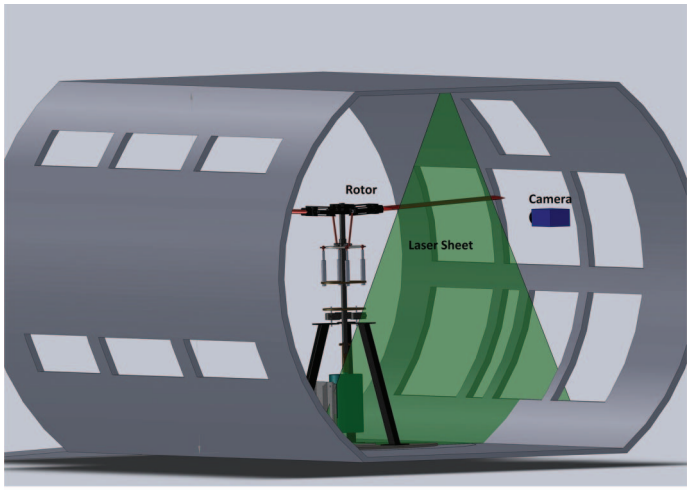

(a) Schematic of the PIV setup for radial flow looking from upstream

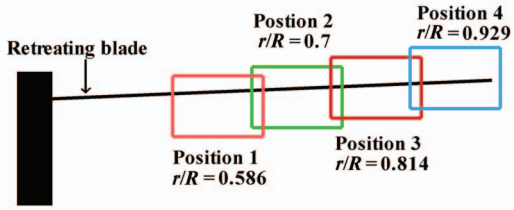

(b) PIV apertures over the radius of the blade

Fig. 3. High Advance Ratio Facility: configured for radial flow.

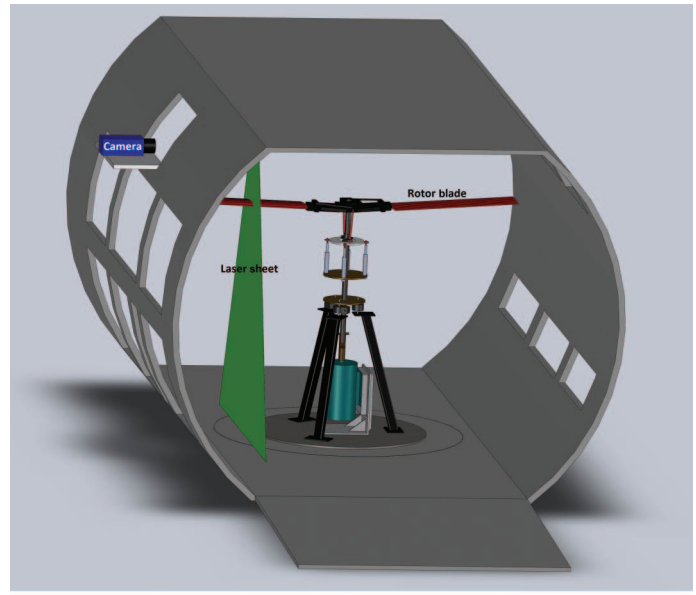

(a) Schematic of the PIV setup for chordwise flow looking from downstream

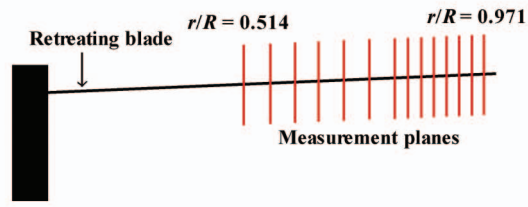

(b) PIV apertures over the radius of the blade

Fig. 4. High Advance Ratio Facility: configured for chordwise flow.

The forward flight rotor results presented here started with extensive PIV studies of the radial velocity field over the retreating blade of a two-bladed teetering rotor in forward flight (Ref. 20). PIV was primarily used to study the radial flow over the dynamically stalled blade in forward flight using the setup depicted in Fig. 3(a). Radial flow measurements were obtained at four stations using the apertures shown in Fig. 3(b). To demonstrate the validity of the radial flow results, static stall tests were conducted on the blade at an angle of attack of 13.5° and a freestream velocity of 15 ft/s (4.6 m/s). Velocity measurements in chordwise axial planes were made at 12 locations between $r/R = 0.514$ and 0.971 with spatial resolution increasing toward the tip, as shown in Figs. 4(a) and 4(b). At each position, a calibration board was used to quantify spatial coordinates. Corrections for the tilt of the laser-illuminated measuring window with respect to the camera image plane were incorporated into the DaVis software.

PIV considerations

The equipment used with the LaVision setup included a New Wave Research Solo Nd:YAG laser, an ImagerIntense charge-coupled device (CCD) camera, and the DaVis imaging software. The laser was double pulsed and frequency doubled to produce 532 nm visible light. The resulting beam diameter was about 3.5 mm with a pulse width of 5 ns. The ImagerIntense camera had a 1376 (h)×1040 (v) pixel viewing area. The scan rate of the CCD sensor was 16 MHz. The focal length of the lens system was 50 mm. The aperture of the camera was set at $f/4$. One hundred image pairs were captured at each measurement location.

Since the mean flow direction was normal to the image plane, it was important to choose a pulse separation (Δt) that was short enough to ensure that the out-of-plane movement did not exceed 1/3 of the sheet thickness as discussed in Ref. 31. A delay of 100 μs was chosen to produce sufficient frame-to-frame particle matching. Accurate PIV measurements also depended on the interrogation window size. The signal-to-noise ratio begins to degrade if particle displacements exceed one quarter of the interrogation window (Ref. 31). Optimally, 7–10 particles in each interrogation window are necessary (Ref. 32). Using results by Yang et al. (Ref. 18), a maximum axial velocity of 8 m/s was estimated while the radial velocity was limited to 3 m/s. A 32 × 32 pixel window would be sufficiently large so that particles traveling less than 10.6 m/s would not travel more than eight pixels or one quarter of the total interrogation window.

Velocities were calculated from the spatial cross-correlation of the images. The average particle displacement in each interrogation window was revealed by the location of the highest correlation peak. With the pixel size of the ImagerIntense camera averaging 6.5 μm, the particle size ranged from 1.06 to 1.97 pixels. The optimal particle diameter for digital cross-correlation is approximately 2 pixels.

An interrogation window overlap of 75% and a second interrogation pass with a reduced window size increased the data yield and the signal-to-noise ratio of the correlation peak. Therefore, the first pass utilized an interrogation window of 64 × 64 pixels, whereas a 32 × 32 pixel window was used on the second pass. Postprocessing of the vector images consisted of an applied vector range and a median filter. As erroneous vectors appeared at the edges of the camera-viewing window, these processes greatly reduced this noise. Further details on the experimental methodology are presented in DiOttavio et al. (Ref. 20).

Cross-flow plane downstream of trailing edge

The choice of the cross-flow plane and the instant immediately following the passage of the trailing edge enabled the capture of the velocity field just above and below the trailing edge without the blade surface obstructing or scattering the laser illumination. The flow at that station, measured much less than a millisecond after passage of the trailing edge, is negligibly different from the station immediately before the trailing edge. Certainly, it is recognized that the wake of the blade changes rapidly and the velocity field thus changes within a short distance of the trailing edge. However, recent computational results by Gross et al. (Ref. 33) verify that the change immediately downstream of the blade is insignificant.

Uncertainty estimate

The uncertainty in collective pitch and cyclic pitch angle settings, which were measured using a digital protractor, is 0.05°. The error in measurement of the angle of the tip path plane arises mainly due to the pixel size in image processing, and the uncertainty is 0.035°.

The probability density histograms of the instantaneous velocity data did not reveal peak locking or any other experimental artifact, the highest resolution of velocity being 0.005 m/s. To estimate the particle lag error (which is typically significant in vortical flows), the particle dynamics in PIV was considered. A transient solution for the response time (relaxation time) of the seed particles (10 μm) to changes in velocity was determined. The characteristic time was defined as the time available for the seed particle to respond to rapid changes in the flow. This was determined from the vorticity contours of the experimental results. A comparison showed that the characteristic time was 5–10 times the relaxation time, indicating that the particle lag error was insignificant. However, this does not allow measurement interpretation from within the boundary layer as the vorticity in the boundary layer is an order of magnitude greater.

In addition, a random error was computed by using Eq. (1) from Ref. 31, where σ_e is the random error, d_p is the particle image diameter, and c is an empirical constant that usually lies between 0.05 and 0.10:

$$\sigma_e = c \times d_p \tag{1}$$

Thus for this experiment the random error ranged from 0.053 in the best case (0.05 $\times$1.06 pixels) to 0.197 in the worst case (0.10 $\times$1.97 pixels).

The total measurement error, ϵ_m, was quantified with Eq. (2) from Ref. 34, where W_p is the maximum out-of-plane component of flow velocity, U_p is the maximum inplane component of flow velocity, Z_s is the light sheet thickness, M is the magnification, and σ_i is the random measurement error in the image plane:

$$\epsilon_m \leq \frac{W_p}{U_p} \times \frac{3}{Z_s M} \times \sigma_i \tag{2}$$

W_p was measured in the chordwise plane and was found to be 2.5 m/s, U_p was measured to be 3.5 m/s, Z_s was maintained between 3 and 4 mm, and M of the camera was 1/16. σ_i amounted to $6.5 \times 10^{-6} \times \sigma_e$ ranging between 3.45×10^{-7} and 1.28×10^{-6}.

Using these relations, the total measurement error ϵ_m was estimated between 0.34% and 1.25%. This amounted to an absolute error of 0.012 and 0.043 m/s based on U_p. Uncertainties in the measurement are summarized in Table 2.

Table 2. Summary of errors

Type of error	Estimate	Error
Random	Eq. (1)	0.053–0.197 pixels
Bias	Peak locking histogram	0.005 m/s
Lag	Relaxation time	Insignificant
Total measurement	Eq. (2)	0.34–1.25%

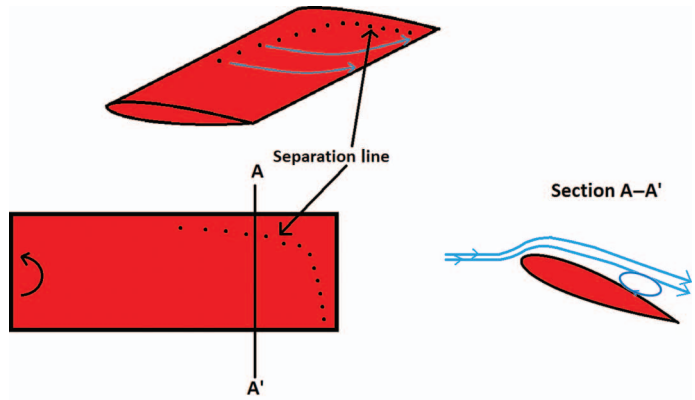

(a) Conceptual representation of the separation line and separated flow

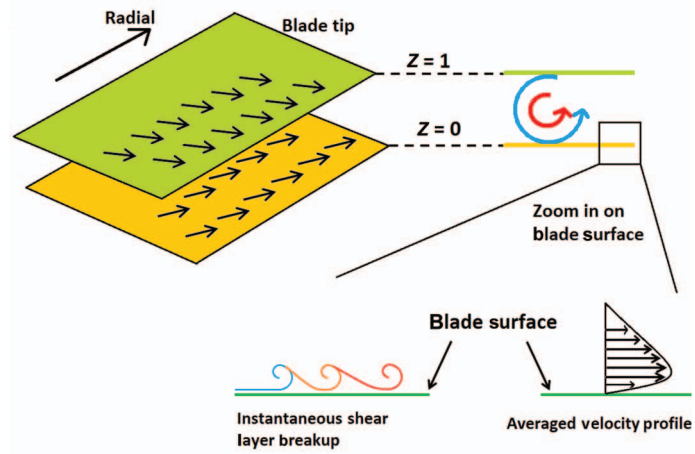

(b) Conceptual representation of shear layer and vorticity above the blade

Fig. 5. Hypothesized flow features on a dynamically stalled rotating blade.

Hypothesized Flow Features

The conceptual flow field is illustrated in Fig. 5. In Fig. 5(b), the $Z = 0$ plane represents a plane immediately above the blade surface and $Z = 1$ plane represents a plane farther above the blade surface. From the prior experimental results, the flow field in dynamic stall is hypothesized to have the following characteristics:

1) The flow downstream of the separation line over the blade is highly three dimensional, and the Mach number remains low in the region downstream of the separation line.

2) The nature of the separation line on a rotating blade will involve interaction between the stall line, tip vortices, and the separated flow field downstream (see Fig. 5(a)).

3) As the flow adjacent to the blade in the separated region moves at low speed relative to the rotating blade, the radial stresses at the surface may be transported to a substantial height above the surface into this flow, in contrast to the case of attached flow (see Fig. 5(b)).

Using these results, the following characteristics of the flow can be hypothesized:

1) The occurrence of a large radial flow can in turn have a strong influence on the separation process itself and thus have a role in determining the shape of the separation line (see Fig. 5(a)).

2) The near-surface flow field will form a radial jet both above and below the blade surface due to the radial acceleration on the surface.

3) This jet will itself be highly vortical as the flow at the blade surface obeys the zero-slip condition with respect to the rotating blade, while the flow immediately above that layer is accelerated radially outward (see Fig. 5(b)).

4) The vortical jet is highly susceptible to shear layer instability due to the unsteady nature of the flow leading to break up of this layer.

From the above, it can be concluded that not just the magnitude and profile of the radial velocity field in this region are of interest. Equally important are the characteristics and behavior of this radial jet, which might contribute to the poststall evolution of lift and pitching moment.

Results and Discussion

Radial flow

The radial flow over the rotor occurs as a result of centripetal and reactive centrifugal forces due to rotation, irrespective of blade stall. The influence of the centrifugal reactive or pumping force could be significant in adverse pressure gradients where the flow is retarded (Ref. 14). Although three-dimensional flow separation can itself manifest as fluctuations in spanwise flow, there exists no physical mechanism to develop a sustained flow in the radial direction due to three-dimensional separation alone. The radial flow characteristics are discussed in detail in the following sections.

Profiles of radial velocity. As hypothesized, the rotation of the blade gives rise to a radial jet flow that develops over the surface. However, the no-slip condition must apply at the blade surface and thus a viscous boundary layer exists. Moreover, the attached flow at the bottom surface of the blade also experiences the same radial acceleration. Therefore, the radial flow velocity field should show radial jet layers adjacent to both the upper and lower blade surfaces. It is also noted that this boundary layer is very thin, and it is not expected that PIV will resolve this in the present experiments. Owing to these reasons, the double-peaked radial velocity profile adjacent to the blade surface appeared as a single peak at the middle of the blade thickness. This was observed at all the radial stations in Fig. 6. It shows that the radial jet is confined to the region close to the blade. The jet appears to exist above and below the blade trailing edge. This is due to the fact that the measurement was taken 2 mm downstream of the trailing edge, as indicated in the discussion regarding the inability to capture the blade boundary layer. For the moment, it can be assumed that the peak of the jet is what is seen but that the radial velocity must drop from the maximum value to zero in the distance between the peak location and the surface of the rotor. This assumption is used to estimate the vorticity in the boundary layer above the blade. For the moment, the phenomena on the bottom surface of the blade are ignored.

The steps that went into producing the plots of radial velocity are, first, the velocity vectors were ensemble averaged; second, using image processing, the blade surface is located from images of laser sheet visualization; finally, the radial velocity component is transformed so that it is parallel to the blade surface (the blade is flapped up $+4^\circ$) to consider the vorticity in the boundary layer.

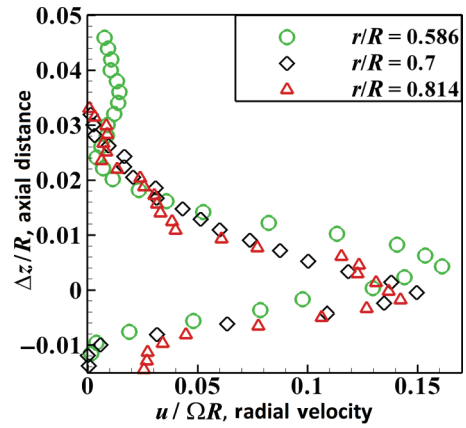

Fig. 6. Profile of the variation of average radial velocity at various radial locations, normalized with respect to blade tip speed.

Figure 6 shows the axial variation of the averaged radial velocity profiles normalized by blade tip speed. The salient feature is that the magnitude of the radial velocity peak essentially decreases on moving outboard along the blade, quite the opposite of the expected increase in radial velocity. The uncertainty in the peak value due to spatial resolution is estimated to be less than 0.61% of the peak height of the velocity profile. The error was estimated by extrapolating the data after ignoring the peak to obtain an extrapolated peak and then comparing it to the measured peak.

Discrete structures in the cross-flow plane. A literature review on the separated flow over lifting surfaces revealed studies on stalled fixed wings, but very little on dynamic stall in flows over "true" rotating blades. Three-dimensional flow patterns were detected on airfoils based on surface visualizations by Gregory et al. (Ref. 35) and surface oil streaklines by Winkelmann and Barlow (Ref. 36). Weihs and Katz in Ref. 37 reported cells in the poststall flow field over straight wings. Similarly coherent structures and cells in the separated flow were observed by Yon in Refs. 38 and 39. Yon also reported the fluctuations attributed to these cells in the wake of a stalled rectangular wing. Low-frequency oscillations were observed in the case of two-dimensional leading edge separation by Broeren and Bragg (Ref. 40). Spanwise separation cells were seen to arise from trailing-edge separation, but this was primarily steady. Thus, from the above discussion it appears that spanwise cells have been observed in the stalled flow over fixed wings, even on nominally two-dimensional airfoil models. However, they are driven by the shear at the top of the separated flow region, which is the only source of vorticity in that situation once the flow is separated. This is very different from the case of a rotating blade where high shear stress in the form of radial stresses is present at the blade surface. In addition, recent numerical studies on a S822 wind turbine airfoil (Ref. 33) showed the effect of cross-flow on a rotating blade. The blade rotation resulted in a radial velocity component toward the blade tip in the separated flow region. The study postulated the existence of stationary and traveling cross-flow vortices over the span of the blade.

Figure 7 shows the vorticity contours in the cross-flow plane at two radial locations in the trailing edge plane. Clearly, the jet shear layer has broken into several discrete structures in the windows shown. In addition, the vorticity entrained in the structures increases on moving outboard. Furthermore, the structures also appear to be lifting off the surface (referred to as "peel" or "jump" off) at the more outboard locations, a

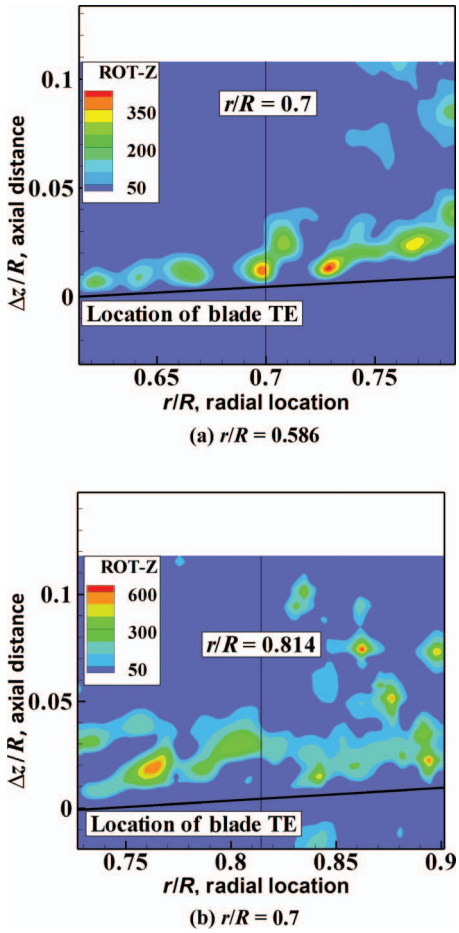

Fig. 7. Contours of vorticity showing discrete structures above the blade.

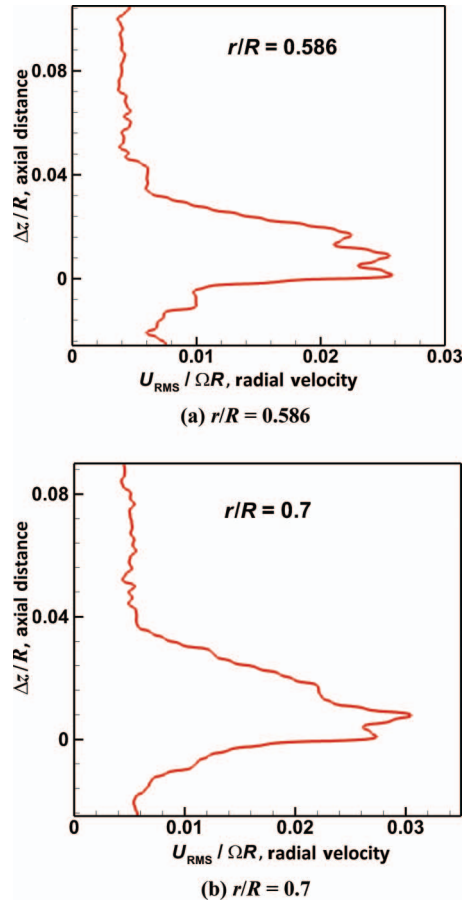

Fig. 8. RMS fluctuations showing the peak occurring near the blade surface.

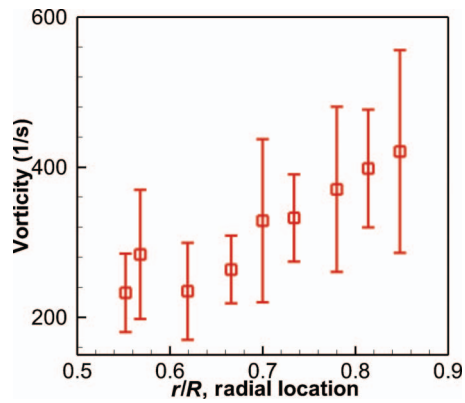

Fig. 9. Radial variation of the average vorticity of discrete structures and their rms variation in the trailing edge plane.

trend also seen in the measurement window centered at $r/R = 0.814$ and beyond (not shown).

To further understand the characteristics of these discrete structures, a statistical convergence test was performed on the data set. This sought to determine at what point during the averaging process would the discrete structures coalesce. First, all the hundred vector fields collected at a given station were averaged. The vorticity of the discrete structures was observed to reduce to the local average vorticity level. Furthermore, after averaging approximately 17 vector fields these discrete structures were no longer distinctly visible. Distinctly visible was defined as the vorticity entrained in these structures being less than 20% higher than the local vorticity. This indicates a moderately rapid change in the precise locations of the structures but also shows that their locations are not drastically different from one velocity field to the next.

Significance of the discrete structures. The significance of the discrete structures is crucial to the understanding of the radial flow. To explore the significance of these discrete structures, first the question—what is the source of these instabilities?—must be answered. Hence in search for the answer, the root-mean-square (rms) variation of the velocity vectors was investigated. The following hypothesis was made: "If the radial flow near the surface is the source of the instability, the fluctuation intensity in rms should be high in the regions of higher radial flow. Else the fluctuations should be higher at the upper edge of the separated flow." The complete analysis of the ensemble averaged profiles showed that in all cases the rms fluctuation peak essentially overlapped the peak of the radial velocity (Fig. 8 shows the rms peak close the blade surface). A significant implication of this analysis is that the discrete vortical structures are "driven" by the vorticity in the radial jet shear layer and not by the shear layer separating the upper edge of the separated/recirculating flow from the freestream. Moreover, the rms fluctuations increased on moving outboard. This indicates that the fluctuation has a primary relationship to the increasing strength of the structures as one moves outboard on the blade.

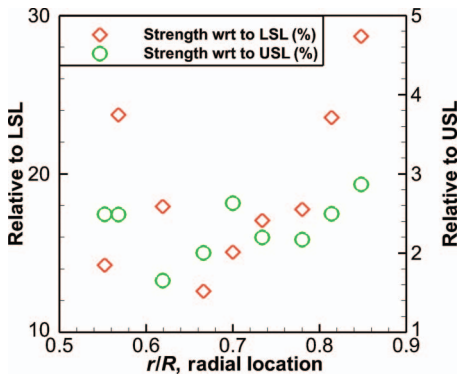

Fig. 10. Average strength of structures with respect to the upper and lower shear layers.

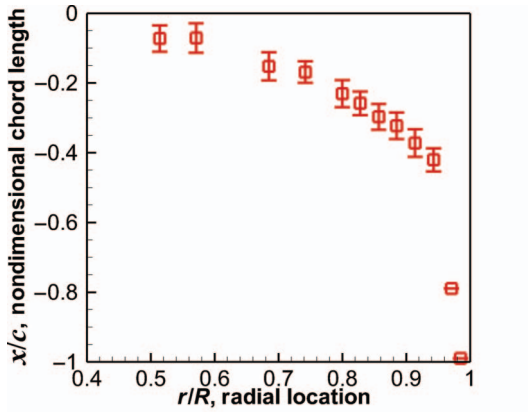

(a) The $x/c = 0$ location is the blade leading edge, whereas $x/c = -1$ is the blade trailing edge

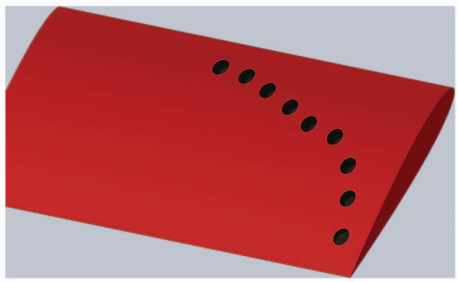

(b) Representation of the separation line on the wing

Fig. 11. Radial variation of the ensemble-averaged separation line, with error bars showing standard deviation.

Quantitative estimates. The average vorticity entrained in the discrete structures at various radial stations is depicted in Fig. 9. The key revelation is that the average strength of the structures and their variance increases on moving outboard on the blade. This fact along with the notion that the discrete structures are "driven" by the radial jet shear layer (discussed in preceding section) can now be used to reconcile the behavior of the radial velocity. In other words, a higher amount of vorticity generated from the surface is entrained in the discrete structures on moving outboard. Subsequently, these discrete structures that were observed to "peel" or "jump" off the blade (see Fig. 7) caused the evident decrease in peak magnitude of the radial velocity on moving outboard on the blade (Fig. 6).

A quantitative comparison of the average strength of the structures to the average vorticity in the shear layers bounding the radial jet is illustrated in Fig. 10. Two shear layers were considered for this analysis. First, the lower shear layer (LSL) is the boundary layer between the solid blade surface and the peak of the radial jet profile. It is produced by the shear between the radially accelerated flow and the no-slip condition at the surface and is the stronger of the two shear layers. Second, the upper shear layer (USL) is the layer of fluid above the point of peak radial velocity. It is produced by the jet velocity decay into the largely stagnant zone above it.

The LSL was observed to be almost an order of magnitude (factors of 7 or 8 have been observed) stronger than the discrete structures at inboard locations. It then weakens, even as the structures themselves get stronger, so that it is only three to four times as strong as the structures at the most outboard locations evaluated. Thus at these outboard locations, the discrete structures carry away 25%–30% of the jet. However, the strength of the individual vortical structures is much less than 2% of the vorticity estimated from the radial velocity profile for the USL. Hence it can be inferred that this jet decay occurs mostly through the breakoff of the discrete structures.

Chordwise flow

The notable feature in the chordwise plane is the location and behavior of the separation line. At each radial station examined, the separation point was determined by plotting the normal velocity 2 mm from the blade surface and determining the point where an abrupt increase in its magnitude was observed. This is a practical way of determining separation from velocity data where resolving the boundary layer itself is impractical. Figure 11 shows the radial variation of the ensemble-averaged separation line with the error bars, showing the standard deviation of the location of the separation point. At inboard locations ($r/R < 0.6$), stall occurred very close to the blade leading edge as seen in Fig. 12, which indicates the severity of dynamic stall. This is a classic feature also observed in other studies (Ref. 4). On the outboard sections of the blade, the separation point moved aft toward the trailing edge. This is attributed to the influence of the downwash induced by the tip vortex.

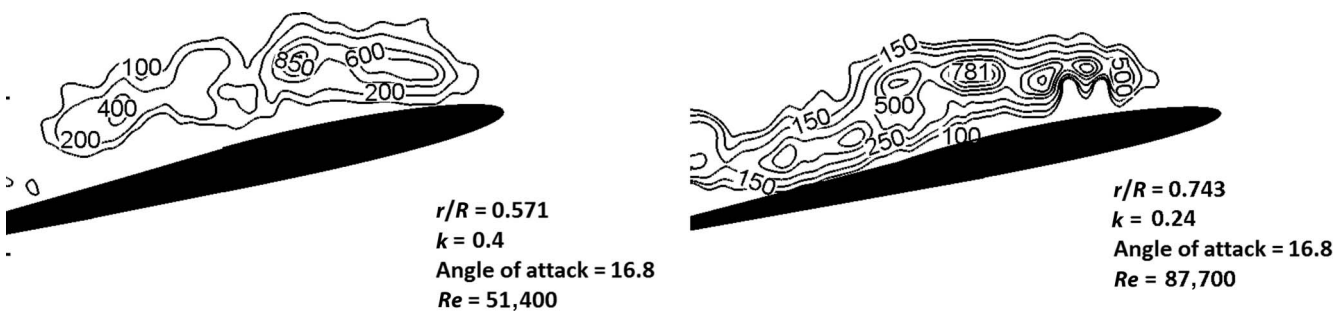

Fig. 12. Instantaneous vorticity observed via PIV at different r/R. (a) Span station, $r/R = 0.571$, (b) span station, $r/R = 0.743$.

The same characteristic is also observed in the vorticity plots where the point of separation moves toward the trailing edge as the radial station of the measurement plane moves outboard. The nonlinear effect of the tip vortex in delay of separation was observed at approximately 50 mm and less from the tip of the blade ($r/R \approx 0.92$). The instantaneous separation line mimics the general trend of Fig. 11, but the line is not smooth as discrete vortices develop within and convect from the separated region as discussed in the section on Radial Flow. This was also illustrated in Raghav et al. (Ref. 19) for a wing in cross-flow.

Conclusions

1) In the separated flow over a rotor blade in retreating stall conditions, the radial velocity along the blade develops a sharp jet-like profile pointing radially outward.

2) Discrete vortical structures occur in the separated flow field immediately above the blade, similar to those breaking off a shear layer.

3) The strongest rms velocity fluctuation in the flow field is near the peak of the radial velocity profile, indicating that the source of vorticity of the discrete structures is the radial jet shear layer rather than the freestream at the upper edge of the separated flow.

4) The discrete vortical structures are observed to "jump" or "peel" off the blade and carry away roughly 30% of the vorticity in the shear layer between the radial jet and the blade surface.

5) The ensemble averaged radial velocity profile data show that the averaged peak radial velocity decreases with increasing radial distance at a given chordwise location, contrary to what would be expected in the absence of the formation and breakup of the discrete vortical structures.

6) From the above, it is concluded that the breaking away of the discrete structures is the mechanism responsible for suppressing the growth of radial jet.

7) Order of magnitude comparisons show that the radial jet development is strength limited by the breakup into discrete structures, and the discrete structures themselves are first-order phenomena in the flow field of the rotor blade in retreating blade stall. These flow characteristics may have significant effects on the evolution of lift and pitching moment of the blade during retreating blade stall.

Appendix: Equations Defining Dynamic Similarity Parameters

1) Tip speed ratio (TSR) was defined as the ratio of local blade speed to the inplane component of velocity to the rotor:

$$\mathrm{TSR} = \frac{\Omega r}{V_c} \tag{A1}$$

2) Angle of attack:

$$V_n = V_w\,(1 - a_o)\cos\gamma \tag{A2}$$

where a_o is a factor that accounts for deceleration of wind due to wind turbine operation (induced velocity):

$$V_c = V_w \sin\gamma \tag{A3}$$

The tangential component of velocity to the blade is a function of the azimuth angle and defined as

$$V_{t_w} = \Omega r + V_c \sin\psi \tag{A4}$$

The angle of attack for the wind turbine blade (α_w) and the rotor setup (α_r) are then defined as

$$\alpha_{i_w} = \arctan\frac{V_n}{V_{t_w}} \tag{A5}$$

$$\alpha_w = \alpha_{i_w} - \alpha_{p_w} \tag{A6}$$

$$\alpha_{i_r} = \arctan\frac{V_i}{V_{t_r}} \tag{A7}$$

where V_{t_r} is the tangential component of velocity to the blade in the rotor setup:

$$\alpha_r = \alpha_{p_r} - \alpha_{i_r} \tag{A8}$$

3) Reduced frequency ($\psi = 270^\circ$):

$$\begin{aligned} k &= \frac{\omega_f c}{2U} \\ &= \frac{\Omega c}{2\,(\Omega r - U_\infty)} \\ &= \frac{c/2r}{(1 - U_\infty/\Omega r)} \end{aligned} \tag{A9}$$

where $\omega_f = \Omega$ for a teetering rotor.

Acknowledgments

The authors gratefully acknowledge support of this work through a grant from the Army Research Office. Dr. Frederick Ferguson is the technical monitor. Valuable input from Professor Marilyn Smith is gratefully acknowledged. Assistance in conducting the experiment by Dustin Teuscher and Felipe Ortega and in data reduction by Akshaya Srivastava is greatly appreciated.

References

[1]McCroskey, W., "Some Current Research in Unsteady Fluid Dynamics—The 1976 Freeman Scholar Lecture," *Journal of Fluids Engineering*, Vol. 99, (1), 1977, pp. 8–39.

[2]Carr, L., McAlister, K., and McCroskey, W., "Analysis of the Development of Dynamic Stall Based on Oscillating Airfoil Experiments," NASA TN D-8382, 1977.

[3]McCroskey, W., Carr, L., and McAlister, K., "Dynamic Stall Experiments on Oscillating Airfoils," *AIAA Journal*, Vol. 14, (1), 1976, pp. 57–63.

[4]McCroskey, W., McAlister, K., Carr, L., Pucci, S., Lambert, O., and Indergrand, R., "Dynamic Stall on Advanced Airfoil Sections," *Journal of the American Helicopter Society*, Vol. 26, (3), 1981, pp. 40–50.

[5]McCroskey, W., McAlister, K., Carr, L., and Pucci, S., "An Experimental Study of Dynamic Stall on Advanced Airfoil Sections. Volume 1: Summary of the Experiment," NASA TM 84245, 1982.

[6]Lorber, P., "Dynamic Stall of Sinusoidally Oscillating Three-Dimensional Swept and Unswept Wings in Compressible Flow," American Helicopter Society 48th Annual Forum Proceedings, Washington, DC, June 3–5, 1992.

[7]Carta, F., "Dynamic Stall of Swept and Unswept Oscillating Wings," UTRC Technical Report ADP005010, 1985.

[8]Koga, D., and Eaton, J., "Active Control of Unsteady and Separated Flow Structures," AFOSR TR 89-1210, 1989.

[9]Larsen, J., Nielsen, S., and Krenk, S., "Dynamic Stall Model for Wind Turbine Airfoils," *Journal of Fluids and Structures*, Vol. 23, (7), 2007, pp. 959–982.

[10]Meunier, M., "Simulation and Optimization of Flow Control Strategies for Novel High-Lift Configurations," *AIAA journal.*, Vol. 47, (5), 2009, pp. 1145–1157.

[11]Van Dommelen, L., and Shen, S., "The Genesis of Separation," Paper A81-32751, Symposium on Numerical and Physical Aspects of Aerodynamic Flows, Long Beach, CA, January 19–21, 1981.

[12]Schreck, S., and Robinson, M., "Blade Three-Dimensional Dynamic Stall Response to Wind Turbine Operating Condition," *Journal of Solar Energy Engineering*, Vol. 127, (4), 2005, pp. 488–496.

[13]Robinson, M., Hand, M., Simms, D., and Schreck, S., "Horizontal Axis Wind Turbine Aerodynamics: Three-Dimensional, Unsteady, and Separated Flow Influences," Third ASME/JSME Joint Fluids Engineering Conference, San Francisco, CA, July 18–23, 1999.

[14]McCroskey, W., and Yaggy, P., "Laminar Boundary Layers on Helicopter Rotors in Forward Flight," *AIAA Journal*, Vol. 6, (10), 1968, pp. 1919–1926.

[15]Schlichting, H., and Gersten, K., *Boundary-Layer Theory*, Springer-Verlag, Berlin, Germany, 2000.

[16]Corten, G., "Flow Separation on Wind Turbines Blades," Ph.D. thesis, University of Utrecht, Utrecht, The Netherlands, 2001.

[17]McCroskey, W., "Measurements of Boundary Layer Transition, Separation and Streamline Direction on Rotating Blades," NASA TN D-6321, 1971.

[18]Yang, J., Balakrishnan, G., and Komerath, N., "Radial Flow Measurements Downstream of Forced Dynamic Separation on a Rotor Blade," AIAA 2006-3377, 36th AIAA Fluid Dynamics Conference and Exhibit, San Fransisco, CA, June 5–8, 2006.

[19]Raghav, V., Richards, P., Komerath, N., and Smith, M., "Three-Dimensional Features of the Stalled Flow Field of a Rotor Blade in Forward Flight." Second International Forum on Rotorcraft Multidisciplinary Technology Proceedings, Seoul, Republic of Korea, October 19–20, 2009.

[20]DiOttavio, J., Watson, K., Cormey, J., Kondor, S., and Komerath, N., "Discrete Structures in The Radial Flow over a Rotor Blade in Dynamic Stall," 26th AIAA Applied Aerodynamics Conference, Honolulu, HI, August 18–21, 2008.

[21]Shipley, D., Miller, M., Robinson, M., Luttges, M., and Simms, D., "Evidence That Aerodynamic Effects, Including Dynamic Stall, Dictate HAWT Structural Loads and Power Generation in Highly Transient Time Frames" NREL/TP 441-7080, 1994.

[22]Shipley, D., Miller, M., and Robinson, M., "Dynamic Stall Occurrence on a Horizontal Axis Wind Turbine Blade" NREL TP 442-6912, 1995.

[23]Veers, P., "The Effect of Aerodynamics Analysis on Fatigue Life Estimation," Wind Turbine Aerodynamics Seminar, Sandia National Laboratories, Albuquerque, NM, March 26–29, 1985.

[24]Huyer, S., Simms, D., and Robinson, M., "Unsteady Aerodynamics Associated with a Horizontal-Axis Wind Turbine," *AIAA Journal*, Vol. 34, (7), 1996, pp. 1410–1419.

[25]Butterfield, C., Simms, D., Scott, G., and Hansen, A., "Dynamic Stall on Wind Turbine Blades," NREL/TP 257-4510, 1991.

[26]Coton, F., Wang, T., and Galbraith, R., "An Examination of Key Aerodynamic Modelling Issues Raised by the NREL Blind Comparison," *Wind Energy*, Vol. 5, (2–3), 2002, pp. 199–212.

[27]Bousman, W., "A Qualitative Examination of Dynamic Stall from Flight Test Data," *Journal of the American Helicopter Society*, Vol. 43, (4), 1998, pp. 279–295.

[28]Bousman, W., "Evaluation of Airfoil Dynamic Stall Characteristics for Maneuverability," *Journal of the American Helicopter Society*, Vol. 46, (4), 2001, pp. 239–250.

[29]Carr, L., and Chandrasekhara, M., "Compressibility Effects on Dynamic Stall," *Progress in Aerospace Sciences*, Vol. 32, (6), 1996, pp. 523–573.

[30]Chandrasekhara, M., Carr, L., and Wilder, M., "Interferometric Investigations of Compressible Dynamic Stall over a Transiently Pitching Airfoil," AIAA 93-0211, 31st AIAA Aerospace Sciences Meeting & Exhibit, Reno, NV, January 11–14, 1993.

[31]Prasad, A., "Particle Image Velocimetry," *Current Science*, Vol. 79, (1), 2000, pp. 101–110.

[32]Adrian, R., "Twenty Years of Particle Image Velocimetry," *Experiments in Fluids*, Vol. 39, (2), 2005, pp. 159–169.

[33]Gross, A., Fasel, H., Friederich, T., and Kloker, M., "Numerical Investigation of Rotational Augmentation for S822 Wind Turbine Airfoil," *Wind Energy*, Vol. 15, (8), 2012, pp. 983–1007.

[34]Raffel, M., Richard, H., Ehrenfried, K., Van der Wall, B., Burley, C., Beaumier, P., McAlister, K., and Pengel, K., "Recording and Evaluation Methods of PIV Investigations on a Helicopter Rotor Model," *Experiments in Fluids*, Vol. 36, (1), 2004, pp. 146–156.

[35]Gregory, N., Quincey, V., O'Reilly, C., and Hall, D., "Progress Report on Observations of Three-Dimensional Flow Patterns Obtained during Stall Development on Aerofoils, and on the Problem of Measuring Two-Dimensional Characteristics," Technical Report CP no. 1146, Aeronautical Research Council, Great Britian, 1971.

[36]Winkelman, A., and Barlow, J., "Flowfield Model for a Rectangular Planform Wing Beyond Stall," *AIAA Journal*, Vol. 18, (8), 1980, pp. 1006–1008.

[37]Weihs, D., and Katz, J., "Cellular Patterns in Poststall Flow over Unswept Wings," *AIAA Journal*, Vol. 21, (12), 1983, pp. 1757–1759.

[38]Yon, S., "Coherent Structures in the Wake of a Stalled Rectangular Wing", Ph.D. thesis, University of California, San Diego, and San Diego State University, San Diego, CA, 1995.

[39]Yon, S.,and Katz, J., "Cellular Structures in the Flow over the Flap of a Two-Element Wing," *Journal of Aircraft*, Vol. 35, (2), 1998, pp. 230–232.

[40]Broeren, A., and Bragg, M., "Spanwise Variation in the Unsteady Stalling Flowfields of Two-Dimensional Airfoil Models," *AIAA Journal*, Vol. 39, (9), 2001, pp. 1641–1651.